EXPERIMENTAL 30-DAY FORECASTING AT GFDL

K. Miyakoda, J. Sirutis, and T. Knutson
Geophysical Fluid Dynamics Laboratory/NOAA
Princeton University,
Princeton, U.S.A.

Summary: This is the report of the 30-day forecast experiment
conducted at GFDL. The first part is a summary of 8 January case
studies, using a finite difference GCM without the anomalous boundary
forcings of sea surface temperature(SST). The experiment reveals that the
forecast skill of 10-day mean variables is marginal at the end of a month,
but that the removal of systematic bias (climate drift) from the original
forecasts raises the skill scores appreciably, producing useful one-month
prognoses. However, the climate drift is alarmingly large; for example,
the forecast error for the 500 mb geopotential height due to the drift is
64% of the total root mean square error. The second part of the paper
discusses the forecasts incorporating the observed SST instead of the
climatological SST. A series of forecasts was carried out for the most
dramatic El Niño event of January 1983. In this study, forecasts were
improved for the tropics by using the observed SST, whereas the impact for
the extratropics was not beneficial. Four possible causes for the adverse
effect of tropical SST were examined, i.e. the cumulus parameterization,
the accuracy of SST, the initialization, and the tropical land surface
condition. Preliminary investigations suggest that the forecast
tropical divergence fields are quite different from those observed , in
particular with respect to the components of large scale divergence
associated with the 40-50 day oscillation. It is likely that the current
initialization of the GFDL forecast system is deficient in treating this
distinct tropical oscillation.

1.   INTRODUCTION

In the past ten years, 30-day forecast experiments have been conducted at
the Geophysical Fluid Dynamics Laboratory (GFDL). The main issues are:
1) whether 30-day forecasts are feasible, and 2) how sea surface
temperature (SST) information can be utilized for monthly forecasts.

Two papers will be summarized in this report. One paper (Miyakoda et al.,
1986) discusses the current skill of the 30-day forecasts based on a
particular general circulation model (GCM) which was frozen in 1980 and
had been applied to 8 January cases until 1985. The other
paper (Sirutis et al., 1986) concerns the effect of SST on the extended
range forecasts for the case of the 1982/83 El Niño event.

Associated with the forecast impact of observed SST, the transition from
the 4-dimensional analysis to the prediction appears to be relevant and
crucial to a proper representation of the tropical 40-50 day oscillation.
In this regard, part of a paper by Knutson and Weickmann (1986) is also
quoted.

2.   EXPERIMENT WITHOUT ANOMALY BOUNDARY FORCINGS

30-day forecasts have been carried out for 8 January cases using a GCM.
Each case is composed of 3 stochastic integrations, starting from three
different initial conditions.

The GCM is a GFDL finite difference model of N48L9-E, which denotes a
lateral resolution of N48 (i.e., 1.875° grid size in the meridional
direction),a vertical resolution of nine levels, and the E-physics. The main
processes of the E-physics are: moist convective adjustment, turbulent
closure scheme, and similarity theory boundary layer fluxes.

The 8 January cases consist of 8 separated 30-day periods, beginning at the initial times of 1 January 1977-83 and 16 January 1979. The initial conditions are generated by the 3 analyses based on the 4-dimensional data assimilations of GFDL, NMC, and ECMWF. In these forecast experiments, the lower boundary condition is prescribed as the climatological SST.

Figure 1 displays the stochastic forecasts based on the 3 initial conditions, i.e., A (GFDL), B (NMC), and C (ECMWF) analyses. The maps show the 500 mb geopotential height prognoses averaged for the last 20 days of the forecast for the 1983 case.
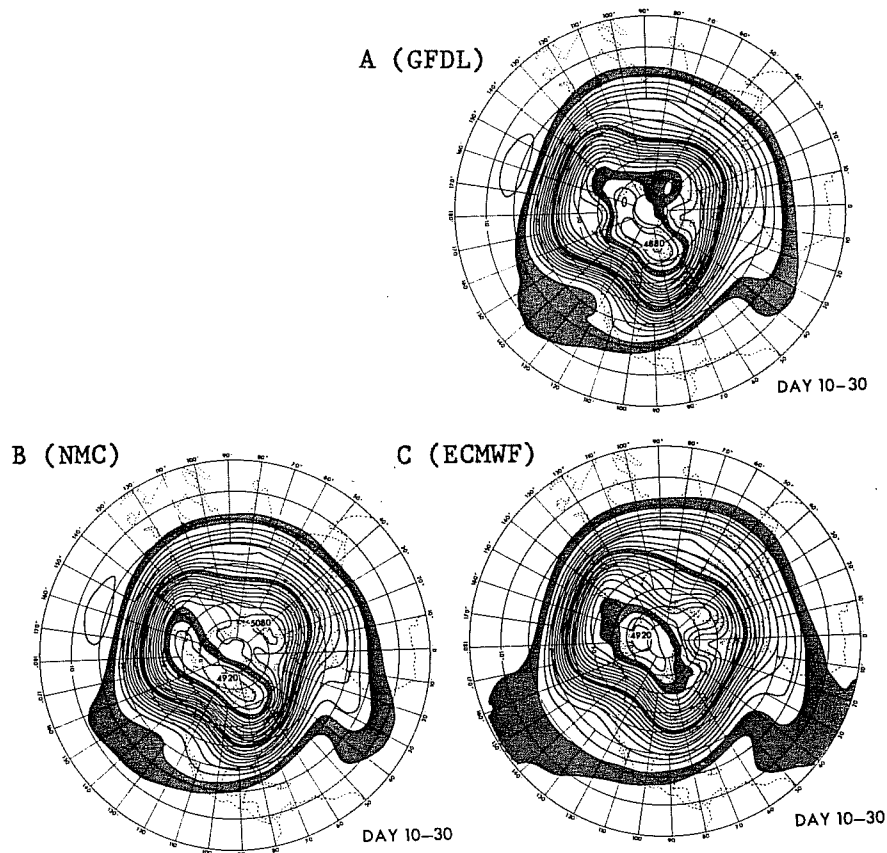

Fig. 1 Three individual forecasts of 20-day mean (Day 10-30) 500 mb geopotential height from (A) GFDL, (B) NMC and (C) ECMWF analyses for the January 1983 case. Contour interval is 40 meters. The shaded contour belts are 5000-5040, 5400-5440, and 5800-5840 meters.
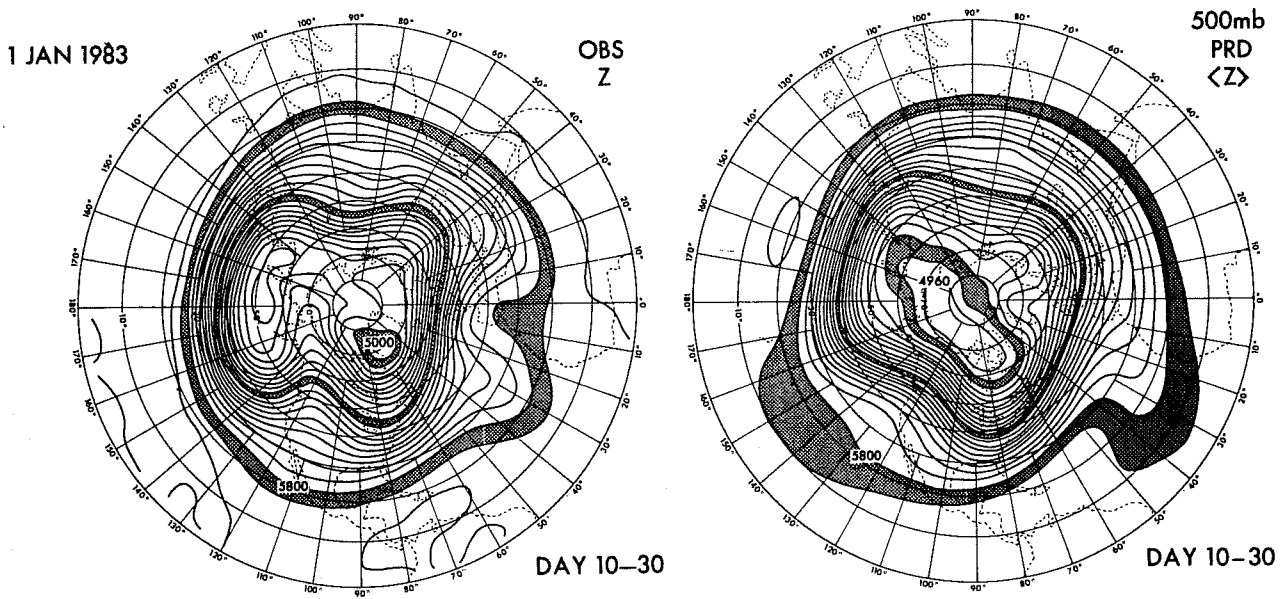
Fig. 2   An example of forecast and observation comparison in the January 1983
        case. The 20-day mean maps of 500 mb geopotential height are shown
        for the observation (left) and the ensemble mean of the three
        forecasts (right). See Fig. 1 for further explanation.

The ensemble mean of the 500 mb geopotential height prognoses over 3

integrations <z> is shown on the right hand side of Figure 2. The

corresponding observed field is shown on the left.

In these figures, it is apparent that (a) the three realizations in Fig. 1

are similar to each other as far as the one-month time-scale is

concerned; they are more similar than is their ensemble mean to the

observation; (b) the predicted geopotential height has lower values in

polar regions than the observation, implying a polar cold bias in the

forecasts; and (c) the blocking ridge over Alaska is of lower amplitude in

the forecast than in the observation.

This is just an example from the 1983 case, but these features are common in

other January cases. These characteristics constitute the systematic

bias (climate drift) of this particular GCM. We will return to this point

later.

The forecast skill scores for the 8 cases are shown in Figs. 3a and 3b. The scores are the root-mean-square errors of the 500 mb geopotential height, Z500, for the northern hemisphere (90°N-25°N). The small circles that are connected with thick solid lines are the rms errors for the 10 day mean forecasts height. The 10 day mean persistence and the 10 day mean climatology are also shown as references. The scores for the 30-day means are plotted on the right hand side of all diagrams. Also displayed in these figures is another curve, i.e., $\sqrt{e_3}$. e_M is the error variance of M-mean Monte Carlo forecast, where M=3 in our case. The definition of e_M is

$$e_M = E\left((\langle z\rangle_M - Z_{obs})^2\right) \qquad (2.1)$$

where Z_{obs} is the observed value, $\langle z\rangle_M$ indicates the mean of z over M samples, and E( ) is the statistical expectation. e_M, therefore, indicates the scatter of forecast errors in the stochastic forecasts due to initial conditions, under the assumption that no systematic bias is included in the forecasting system and the GCM is perfect. Hayashi (1986) showed that e_M is related to the scatter p_1 by

$$e_M = (1 + M^{-1}) \cdot p_1 \qquad (2.2)$$

where

$$p_1 \equiv E\left((z - \langle z\rangle_\infty)^2\right) \qquad (2.3)$$

In Fig. 3, $\overline{p_1}$ is approximated by

$$\overline{p_1} = \sum_{i=1}^{3} \overline{(z_i - \langle z\rangle_3)^2} /(3-1) , \qquad (2.4)$$

where $\overline{(\ \ )}$ is the domain average over the northern hemisphere extratropics (90°N-25°N). Therefore, the plotted values of $\sqrt{\overline{e_3}}$ is

$$\sqrt{\overline{e_3}} = \sqrt{(1 + 1/3)\cdot\overline{p_1}} \ . \qquad (2.5)$$

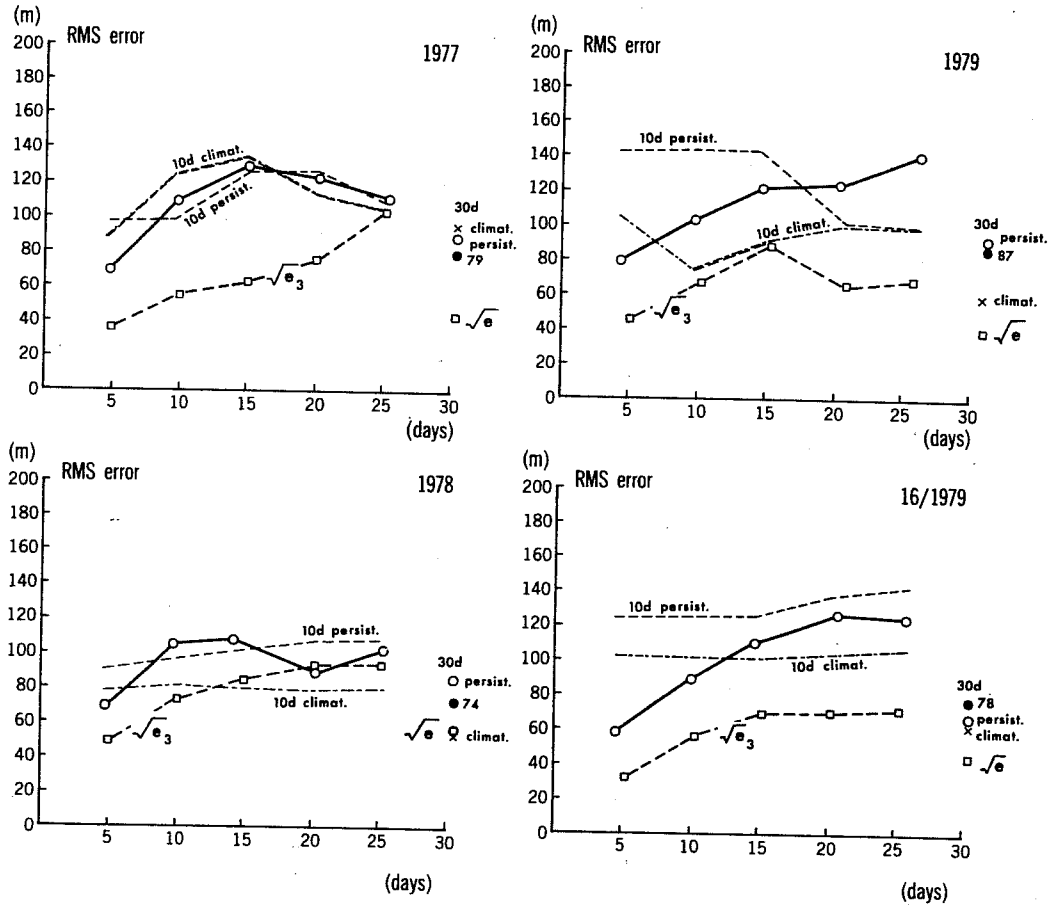Figures 3a and 3b indicate that $\sqrt{\overline{e_3}}$ has reached the persistence

21

Z500mb   NH (90°–25°N)

(m)
200 RMS error   1977

180
160
140   10d climat.
120   10d persist.
100
80   30d
60   √e₃   x climat.
40   O persist.
20   ● 79

0   5   10   15   20   25   30
                              (days)   □ √e

(m)
200 RMS error   1979

180
160
140   10d persist.
120
100   10d climat.   30d
80   O persist.
60   √e₃   ● 87
40
20   x climat.

0   5   10   15   20   25   30
                              (days)   □ √e

(m)
200 RMS error   1978

180
160
140
120   10d persist.
100
80   30d
60   √e₃   10d climat.   O persist.
40   ● 74
20   √e ♀ climat.

0   5   10   15   20   25   30
                              (days)

(m)
200 RMS error   16/1979

180
160
140   10d persist.
120
100   10d climat.   30d
80   ● 78
60   √e₃   O persist.
40   x climat.
20
                                        □ √e
0   5   10   15   20   25   30
                              (days)

Fig. 3a rms error of 500 mb geopotential height in the first four January
cases. Thick solid lines connected with small circles are for the
3-ensemble 10-day mean height. Dotted lines are for the 10-day
persistence and dotted-dashed lines are for the climate departure of
10-day mean height. Thick dashed lines connected with small squares
are the square root of the error variances of three ensemble 10-day
mean forecasts, √e₃, which are derived from the stochastic scatter.
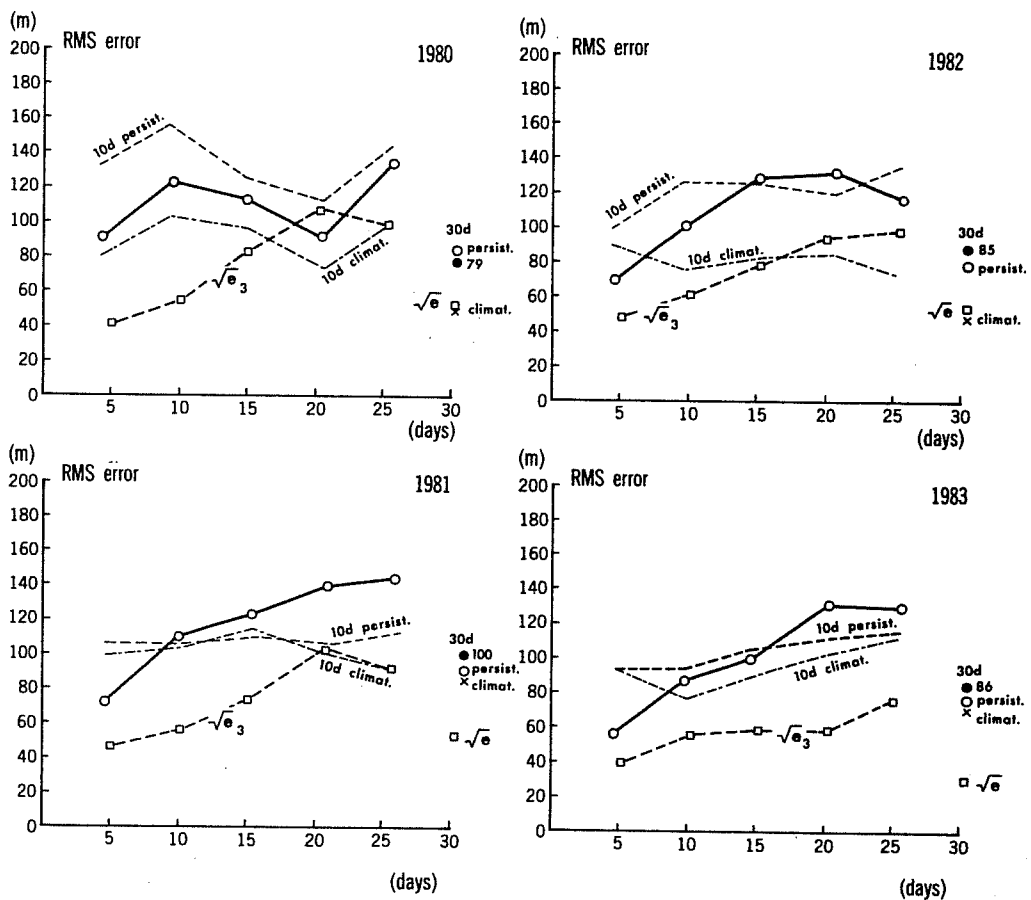
Z500mb   NH (90°-25°N)

Fig. 3b The same as Fig. 3a but in the last four January cases.
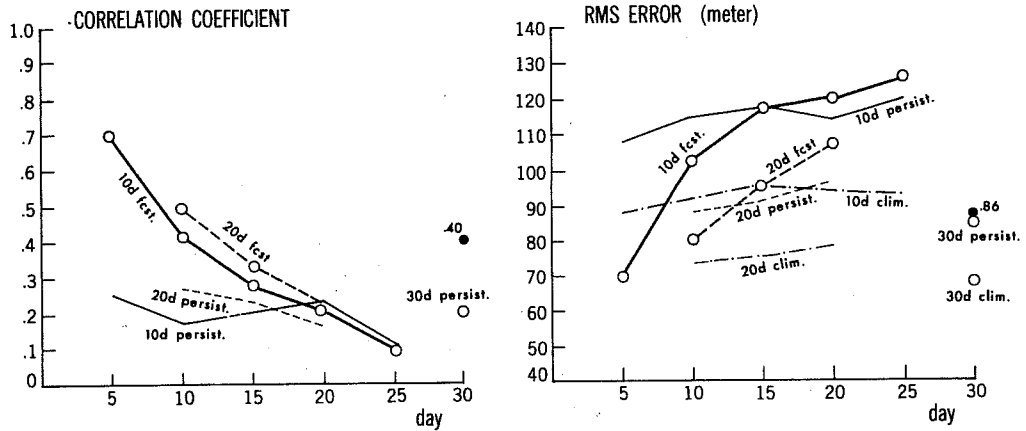
Z 500mb NH (90°-25°N)

Fig. 4 Arithmetic mean skill scores over 8 January cases for 500 mb
geopotential height. Correlation coefficients (left) and rms error
(right). Thick lines connecting small circles are for forecasts and
thin lines are for persistence. Solid and dashed lines are for the
10-day and the 20-day mean height, respectively. The scores for the
30-day mean height are plotted on the right hand side of each diagram.
In the rms diagram, thin dashed-dotted lines are for the climate
departure.
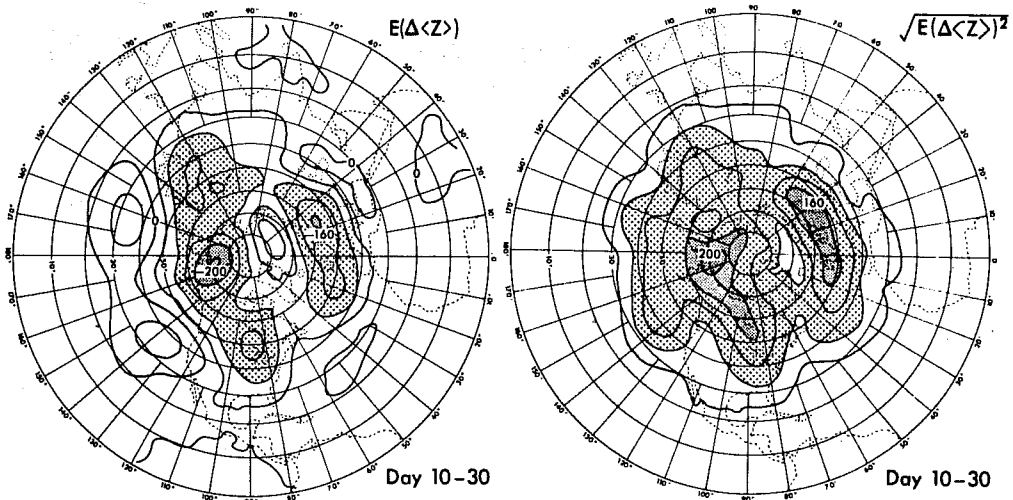
Fig. 5 Eight case average of 500 mb height errors for Day 10-30. Arithmetic
mean error (left), and rms error (right). Contour interval is 40
meters. The areas of lower than 80 meters (in left panel) and of
higher than 80 meters (in right panel) are stippled.

24

level for only two out of 8 cases at the end of a month, and that it has reached the climate levels for four out of 8 cases.

Figure 4 is a summary of the 30-day forecast skill scores of 500 mb geopotential height over 8 January cases. In the correlation coefficient diagram (left), the curves for the 10 day and 20 day mean height decline monotonically, reaching 0.1 at the end of a month. In the rms error diagram (right) the error curves cross the persistence at Day 15, and they cross the climate curves much earlier. This result is not explained by the growth of initial errors and suggests that a great deal of systematic bias is involved in the forecasts. In summary, the monthly forecasts have marginal skill with this GCM.

3.   CLIMATE DRIFT

One of the outstanding features in these forecasts is a large amount of systematic bias. Figure 5 shows two kinds of errors for the 500 mb geopotential height. The left map is the mean error, defined by

$$\text{mean error} = E(\Delta \langle z \rangle) \ , \qquad\qquad (3.1)$$

where

$$\Delta \langle z \rangle = \langle z \rangle_3 - z_{obs}$$

and E is the arithmetic average over 8 January cases. This error is, therefore, the systematic error or the "climate drift." The map on the right is the rms error, defined by

$$\text{rms error} = \sqrt{E(\Delta \langle z \rangle)^2} \qquad\qquad (3.2)$$

In general, the forecast skill is assessed by this error, and therefore the rms error will hereafter be referred to as the "forecast error."

It is intriguing and interesting to note that the rms error on the right is highly correlated with the mean error on the left. In other words, a large portion of the forecast error is due to the climate drift. Figure 6 shows the square of the ratio of the climate drift to the total forecast error, i.e.,

$$(\text{ratio})^2 = \frac{\left\{E(\Delta\langle x\rangle)\right\}^2}{\overline{E(\Delta\langle x\rangle)}^2} \quad , \tag{3.3}$$

where x is an arbitrary variable, $\overline{(\ )}$ is the area average over the northern hemisphere extratropics (90°N-25°S).

For example, 64% of the forecast error of the 500 mb geopotential height for the northern hemisphere for Day 10-30 is due to the climate drift (i.e., .64 = $\sqrt{.41}$). For the temperature error at 300 mb, the climate drift contributes 83% (i.e., .83 = $\sqrt{.70}$) of the forecast error. The ratio is increased for the southern hemisphere and tropics; for example, the systematic bias is 94% (i.e, .94 = $\sqrt{.90}$) for the temperature error in the tropics. The ratio of the climate drift increases steadily with forecasting time range from Day 0-10 to Day 20-30. However, it is not known yet exactly when the drift reaches its asymptote. Another interesting and serious question is whether this systematic error approaches the final asymptote monotonically or whether it overshoots before the final asymptotic value for a brief period.

In the paper by Miyakoda et al. (1986), it was demonstrated that the individual forecasts have been improved by simple subtraction of the climate drift from the prognoses. Figure 7 is the result of the skill scores after this empirical correction. The correlation values have been substantially raised by the climate adjustment. Likewise, the rms errors
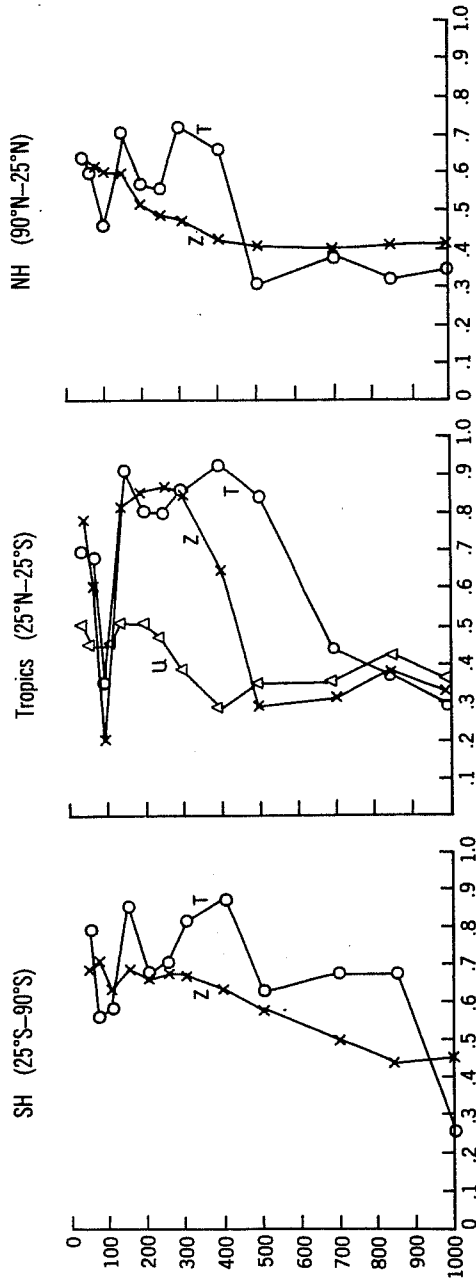
RATIO OF CLIMATE DRIFT TO TOTAL ERROR

Fig. 6 The squared ratio of climate drift to forecast error based on
Eq. (3.3) in the text The values for the geopotential height Z(x),
the temperature T(0), and the zonal component of wind u(Δ) are plotted
as a function of pressure level (mb) for three regions: northern
hemisphere, tropics, and southern hemisphere.

Z500mb NH (90°–25°N)
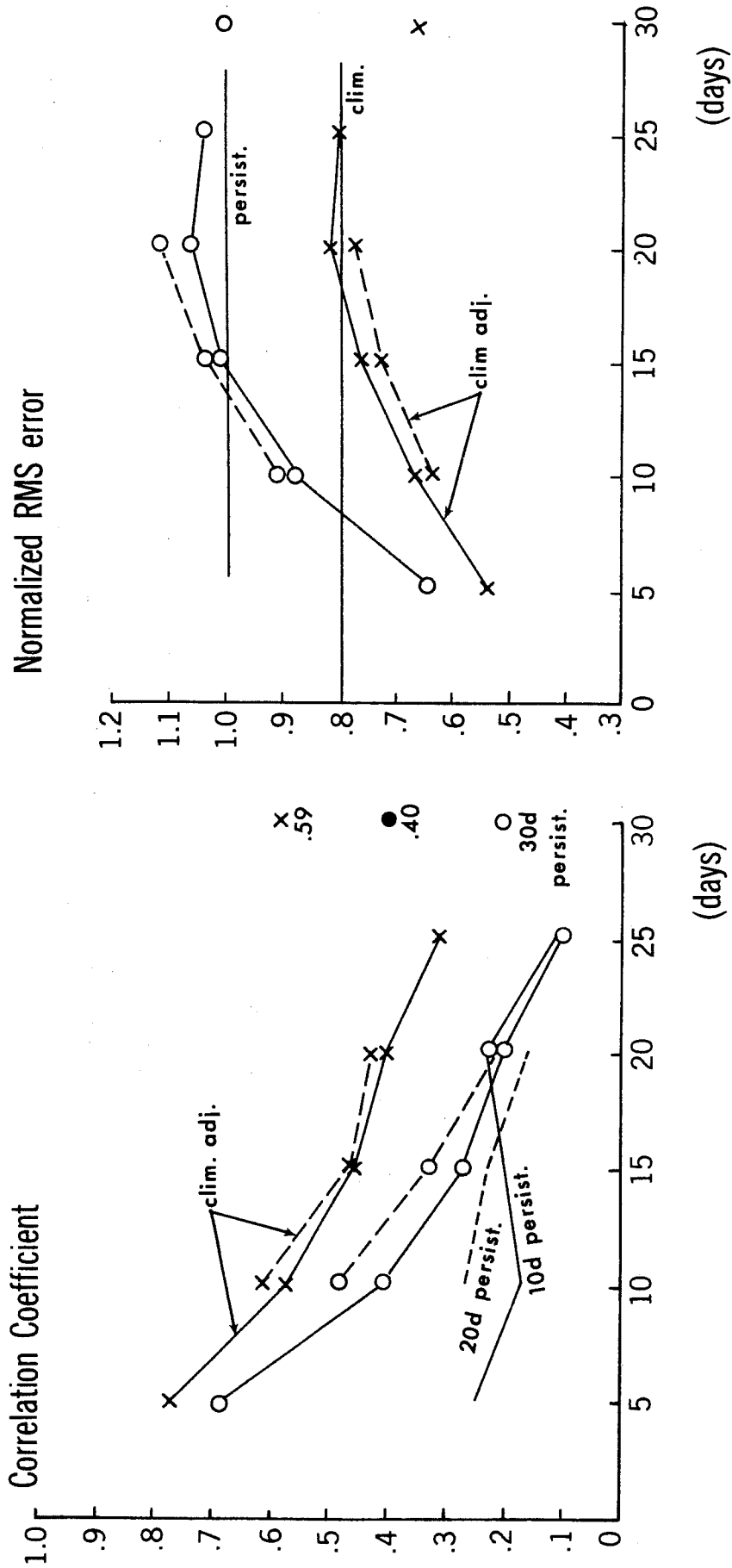
Correlation Coefficient

Normalized RMS error

Fig. 7 Arithmetic mean skill scores over 8 January cases. Correlation
coefficients (left) and normalized rms error (right) for the
stochastic mean of 500 mb geopotential height. The original forecasts
are small circles, and the empirically adjusted forecasts are small
crosses. Solid and dashed lines are for the 10-day and the 20-day
means, respectively. See Fig. 4 for further explanation

28

have been appreciably reduced. The diagram on the right shows the rms error normalized by the persistence. The rms errors both for the 10-day and 20-day means are now below the clim line after the adjustment. It is thus concluded that the climate drift adjustment makes the current monthly forecast results usable. Perhaps more importantly, this diagram suggests that the adjusted level of forecast skill is the attainable level of predictability.

4.   PREDICTABILITY

The probabilistic forecasting system produces two basic prognostic variables, i.e., the ensemble mean and the scatter. The latter is a useful quantitative measure of the likelihood and the reliability of the former. The large scatter implies that the particular gross weather may be less deterministic and less predictable.

It may be interesting to see how the 8-case average of the scatter is distributed geographically. Figure 8 shows $\sigma_f(z500)$, which is defined by

$$\sigma_f(z) = \sqrt{E\langle z - \langle z \rangle \rangle^2} \qquad (4.1)$$

This distinct pattern is similar to the pattern of low frequency (>10-day variability) geopotential height by Blackmon et al. (1977). There are three maxima, i.e., Alaska, the North Atlantic, and the Urals. These maxima correspond to areas where blocking highs frequently occur.

On the other hand, the upper panel of Fig. 9 includes the interannual variability of 500 mb geopotential height, $\sigma_N(z500)$, defined by

$$\sigma_N(z) = \sqrt{E(z - E(z))^2} \quad , \qquad (4.2)$$

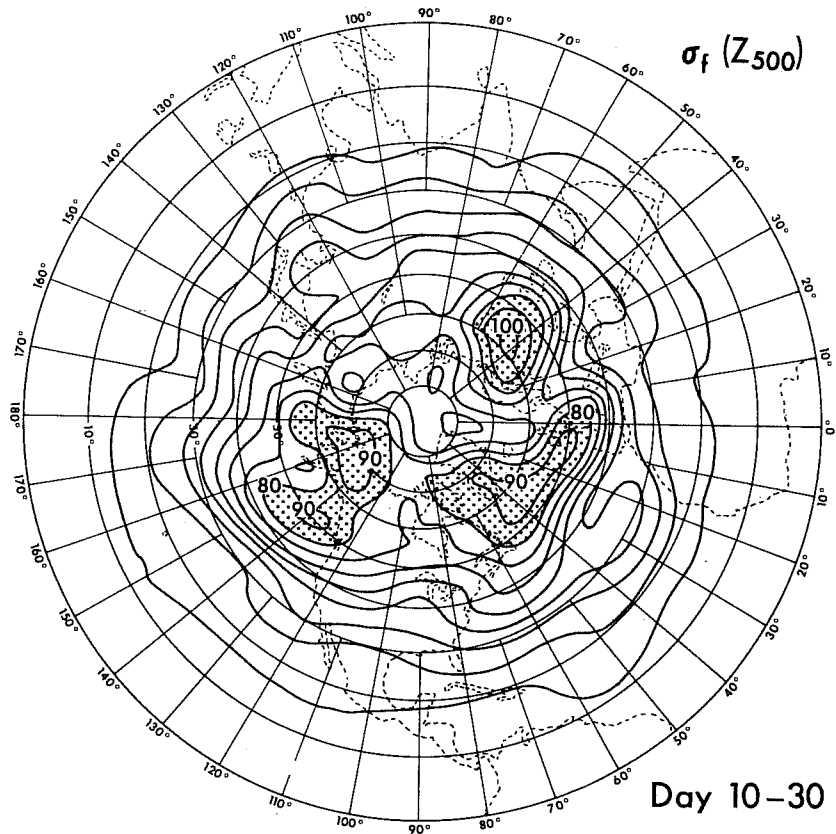Interestingly, but not surprisingly, the pattern of σ_N resembles the pattern of scatter, σ_f, in Fig 8.

Fig. 8 Eight case average of stochastic scatter of geopotential height, σ_f(Z500). Contour interval is 10 meters. The areas of σ_f>80 meters are stippled.

The lower panel of Fig. 9 shows the ratio of σ_f/σ_N. This may be interpreted as indicating the ensemble mean predictability of geopotential height at 500 mb level (Hayashi, 1986). Tentatively it is considered that the areas whose ratio exceeds unity are the unpredictable zones; to be exact, however, $\sqrt{(1+1/3)} = 1.15$ should be multiplied, as was done in association with Eq. (2.2). Figure 9 shows that the potentially predictable zones are distributed over oceans and over the blocking high regions.

A similar pattern was obtained by Shukla (1981) in his pioneering work on monthly mean predictability in which the statistics based on the indices of F-tests were used; Madden (1976) also initiated the potential predictability argument along a similar line. It is noteworthy that the
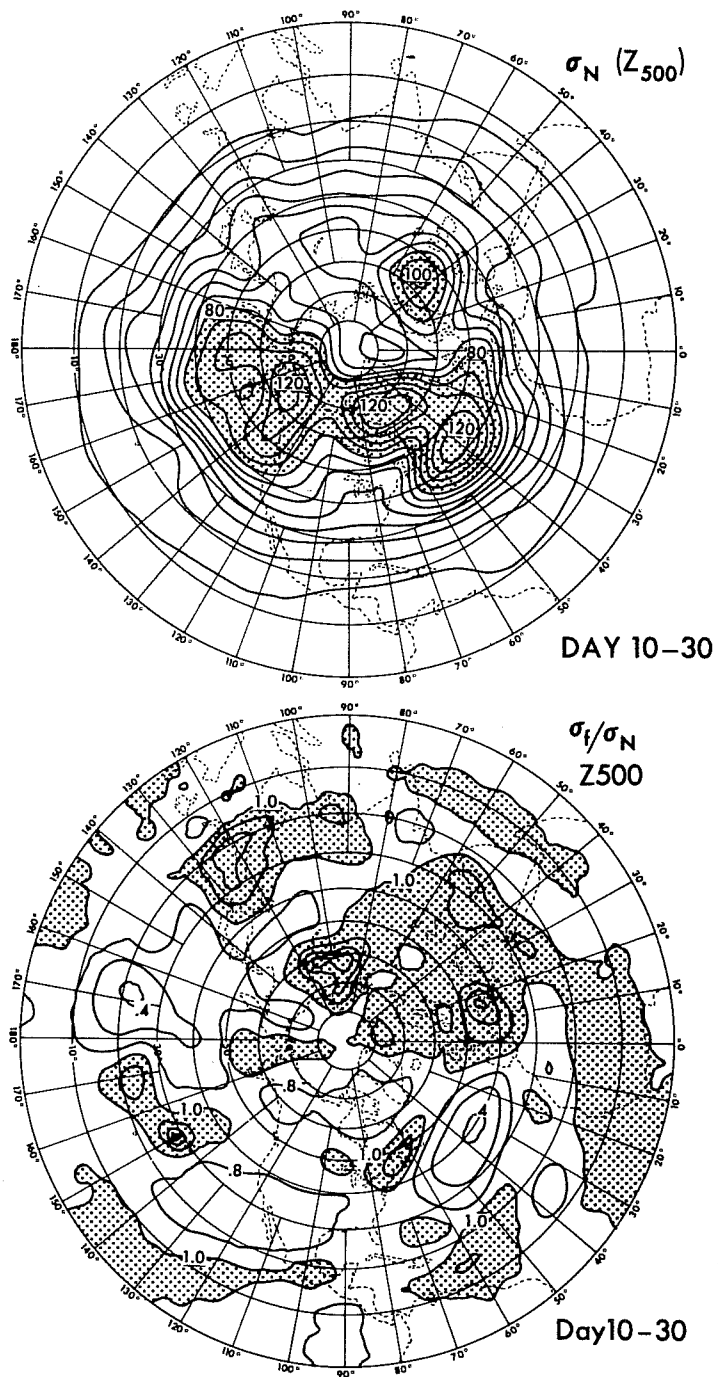
Fig. 9   The interannual variances, $\tilde{\sigma}_N$, (upper) and the normalized scatter, $\sigma_f/\tilde{\sigma}_N$, (lower) for the 500 mb geopotential height, Z500.

$\sigma_N (T_{850})$

DAY 10-30

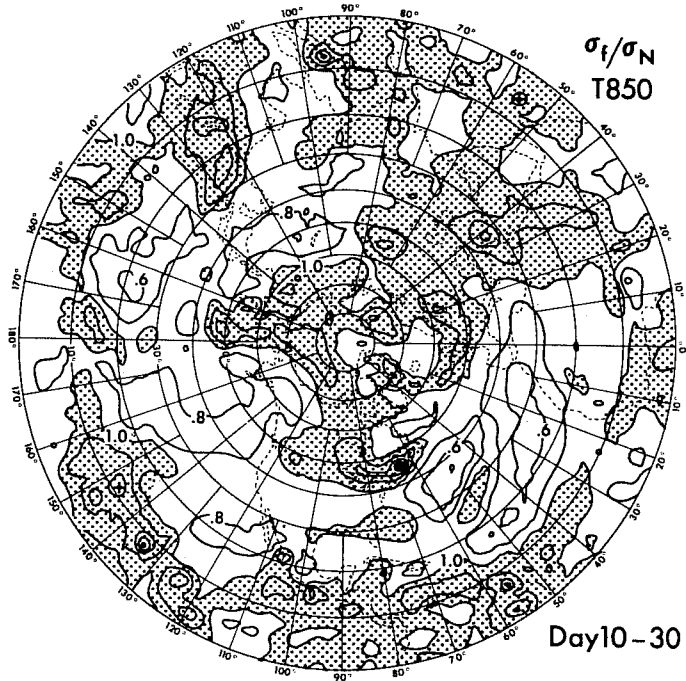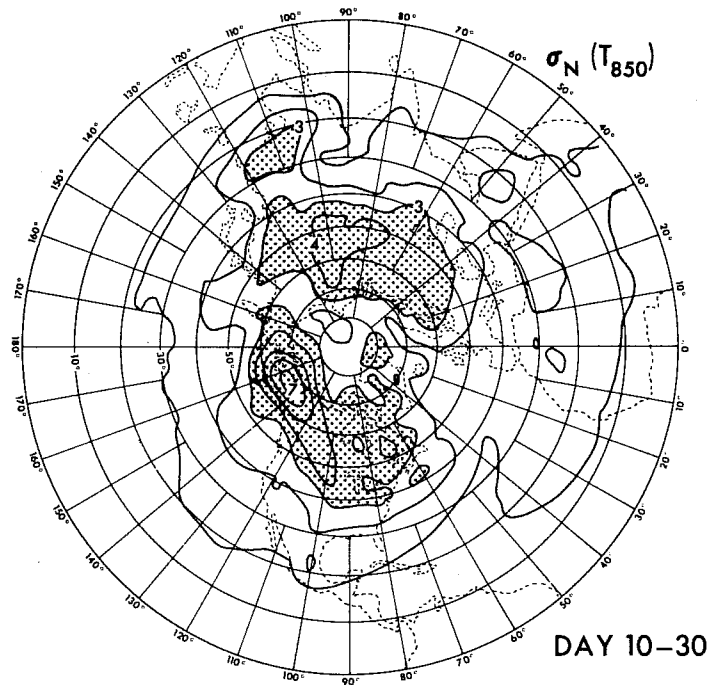σ_f / σ_N

T850

Day10-30

Fig. 10 The same as Fig. 9 but for the 850 mb temperature.

geographical distributions of predictability in all studies have not
agreed well with each other. The disagreement may be due to the different
approaches to the estimate (see also Shukla, 1983) and the insufficient
number of samples.

In summary, <u>predictability</u> <u>regions</u> <u>differ</u> <u>with</u> <u>respect</u> <u>to</u> <u>variables</u> (see
Fig. 10), and presumably with respect to seasons; and <u>the</u> <u>predictable</u>
<u>zones</u> <u>of</u> <u>geopotential</u> <u>height</u> <u>are</u> <u>located</u> <u>over</u> <u>the</u> <u>blocking</u> <u>high</u> <u>regions</u>
<u>and</u> <u>over</u> <u>oceans</u>.

5.   <u>EXPERIMENT WITH ANOMALY BOUNDARY FORCINGS OF SST</u>

It has long been envisaged that the use of the observed SST anomaly may
enhance the forecast skill of extended range forecasts. In particular,
the tropical sea temperature anomaly during El Niño events is so
pronounced that a significant influence must be exerted on the
mid-latitude planetary-scale circulation of the atmosphere (Bjerknes,
1969; Rowntree, 1972; Webster, 1972).
Using the observed SST of Reynolds (1982) for 1977-83, we have carried out
a 30-day forecast experiment using 5 of the 8 January cases. However, the
test results so far do not exhibit an appreciable forecast improvement
over the climatological SST forecasts. We believe, however, that a
positive impact of the SST should be demonstrated if the problem is adequately
treated. This view came from a number of sensitivity experiments such as
Blackmon et al. (1983), Lau (1985), and Kang and Lau (1986). If a long
integration is performed (say 15 years or so), the effect of SST can
be detected with statistical significance even by simple unsophisticated
GCMs. In the GCM solutions of Kang and Lau (1986), it was revealed that
the first EOF mode of atmospheric variability in the extratropics is
highly correlated with the changing SST forcing imposed over the tropical

Pacific. A question is then, what is the adequate treatment of SST in the

framework of dynamical forecasts?

In this situation we have decided to focus our attention on the case of the

1982/83 El Niño because the magnitude of SST anomaly in this case was

unmistakably large, and the effect on large scale weather was very

pronounced. The model adopted in this part of the study is also the

finite difference version of N48L9, and the physics are not only the E but

also the F, the FM, the ES, the FS, and the FMS. An explanation of the

E-physics has been given earlier. The F-physics is the same as the

E-physics, except that the Arakawa-Schubert cumulus parameterization

(Arakawa and Schubert, 1974) replaces the moist convective adjustment, and

that the condensation criteria are 100% humidity in the F and 80% in the

E. The FM-physics is different from the F-physics only in the specified

mountains; the FM uses the "Envelope" mountain of 2 sigma (Wallace

et al., 1983). The ES, the FS, and the FMS are the versions in which the

observed SST is employed.

The results are assessed by the models' performance at forecasting the

streamfunction, ψ, the velocity potential, χ, and the zonal wind, u, in

the tropics (25°N-25°S), and the geopotential height, z, in the

extratropics (90°N-25°N).

6.   RESULTS OF 30-DAY FORECASTS WITH SST ANOMALY

Figure 11 is an example of the skill scores for 30-day forecasts from the

initial time of 00 GMT 1 January 1983. The skill is shown by the

correlation coefficients of χ between the forecasts and the observations

at the 200 mb level over the tropics. In this particular diagram, the

verified data are the NMC analyses. The figures include the scores for 3

34

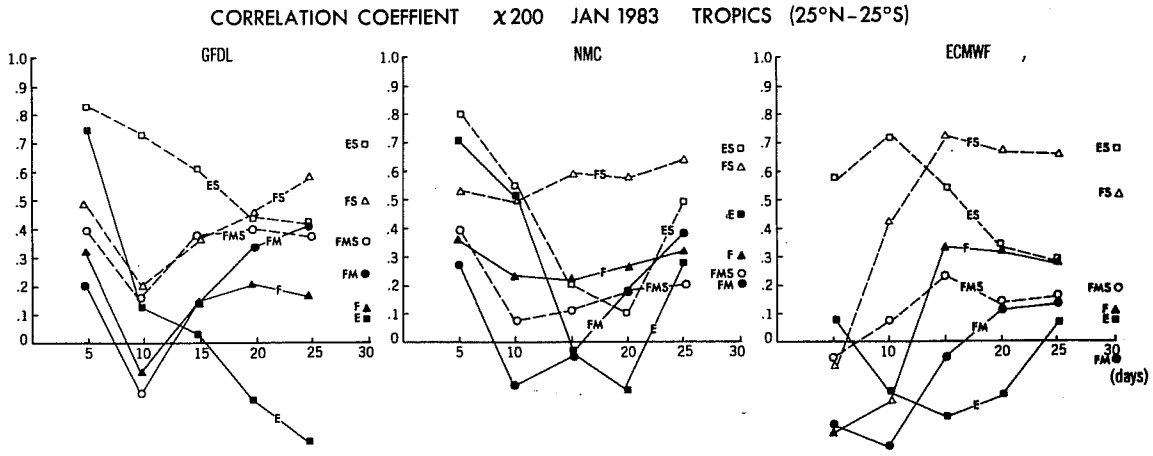CORRELATION COEFFIENT   X200   JAN 1983   TROPICS (25°N-25°S)

Fig. 11 Correlation coefficients of the velocity potential χ at 200 mb between
the forecasts and observations (NMC verification) using 6 models and 3
initial conditions (GFDL, NMC, and ECMWF).

individual forecasts from different initial conditions, i.e., the analyses

of GFDL, NMC, and ECMWF.

The scores of the E, the F, and the FM (with climatological SST) are shown

by the solid lines in Fig. 11, while the scores of the ES, the FS, and the

FMS (with observed SST) are shown by the dashed lines. The scores for the

30-day means are plotted on the right hand side of each diagram. It is

clear from these diagrams that (a) the forecasts with the observed SST are

consistently better than those with climatological SST, and (b) similar

behavior is found in the forecasts from three different initial

conditions. The forecasts from the ECMWF initial conditions appear to

give the worst scores, but this is misleading because the verification is

not performed with the ECMWF analysis.

In order to gain an overview on the performance of various models, Figs.

12a and 12b are prepared to show the score tables à la American

"Consumer Report." The scores in Fig. 12a are based on the correlation

coefficient and those in Fig. 12b are based on the rms error. The ratings

of the ES, the FS, the FMS, the E, the F, and the FM models are made with

35

Fig. 12a The score table of various models and initial conditions based on the correlation coefficients for ψ, χ and u in the tropics.

Fig. 12b The same as Fig. 12a but based on the rms error.

respect to different variables. The variables adopted for this purpose are $\psi 200$, $\psi 850$, $\chi 200$, $\chi 850$, and u850 for three different initial conditions separately, where $\psi 200$, for example, denotes the streamfunction ψ at 200 mb level. The rating is conducted for one variable in a row at one time, and the result is presented using the symbols $\bigcirc$, $\bigcirc$, $\bigoplus$, $\bigcirc$, $\bigcirc$, and $\bullet$, to denote relative performance in descending order. Column I and II indicate the assessment based on the scores of the last 20 day mean and the 30-day mean, respectively, for the correlation coefficient and the rms error. The results using the correlation coefficient and the rms errors are in exact agreement. The overall evaluation summary is given on the bottom row.

It is once again noted that the forecasts with the observed SST are better than those with the climatological SST. The FS-model performs best, the ES is second, and unexpectedly the FMS-model does not perform well. The last point appears to imply that the envelope mountain gives an adverse effect in the case of combined effect with the observed SST in the tropics at the beginning of the forecast.

A serious problem, however, occurs in the extratropics. Figure 13 shows that correlation coefficients of the ensemble mean 500 mb geopotential height anomaly between the forecasts and the observations over the domain of 90°N-25°N. The forecasts with the observed SST gave consistently and significantly worse scores than those with the climatological SST.

Preliminary investigation suggests the following. The reason for the negative SST effect in the middle latitudes is that the tropical heat sources are not exactly at the right places and not of the right magnitude, and consequently the propagating waves from the tropics to the extratropics are distorted.
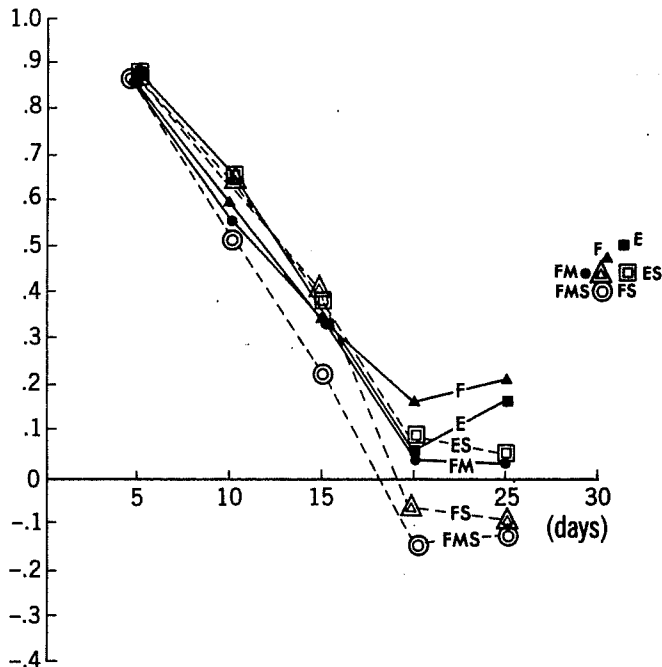
Fig. 13 Correlation coefficients of the three-ensemble and 10-day mean of 500 mb geopotential height anomalies between the forecasts and observations for the northern hemisphere. The scores for the 30-day mean height are plotted at the right hand side.

7. EFFORTS FOR IMPROVEMENT

The causes for the misrepresentation of the tropical heating are under investigation, and the following candidates are mentioned: (a) the initialization of the atmospheric states, (b) the soil moisture over tropical land areas, and (c) the accuracy of the SST. Other than those listed above, the adequacy of cumulus parameterizations has often been questioned. In this study, however, both the E- and the F-physics have been tested, and the results shown already. Our experiment indicates that the misrepresentation occurs with both parameterization methods.

Overviewing the recent SST studies by other researchers, it is noted that successful experiments, using the observed SST and the real initial conditions, are emerging, such as Fennessy et al. (1985), Palmer and

Mansfield (1986), and Cubasch and Wiin-Nielsen (1986). However, a beneficial impact on the extratropical forecast is not always guaranteed, indicating that extreme subtlety is involved in this problem.

Turning back to the candidates for the cause of the deficiency, we have tested item (b) and found that the effect of soil moisture is indeed an important factor for the improvement of forecasts. Concerning item (c), we examined three versions of SST for January 1983 (see Fig. 14). The SST at the top of the figure (SST0) was produced by Reynolds based on ship data alone. The SST in the middle (SST1) by a blending of the ship and the infrared satellite data, also by Reynolds (1983). The SST at the bottom (SST2) is an artificially modified distribution based on the satellite measurements of outgoing long-wave radiation (OLR). In the maps of SST0 and SST1, there is a gap in the SST values at 160°W and 7°S, reflecting the data of a ship lane between Fiji and Hawaii. In the map of OLR, however, a minimum (maximum convective activity) is located exactly at the place of the gap. Thus the modification was made in SST2 so as to
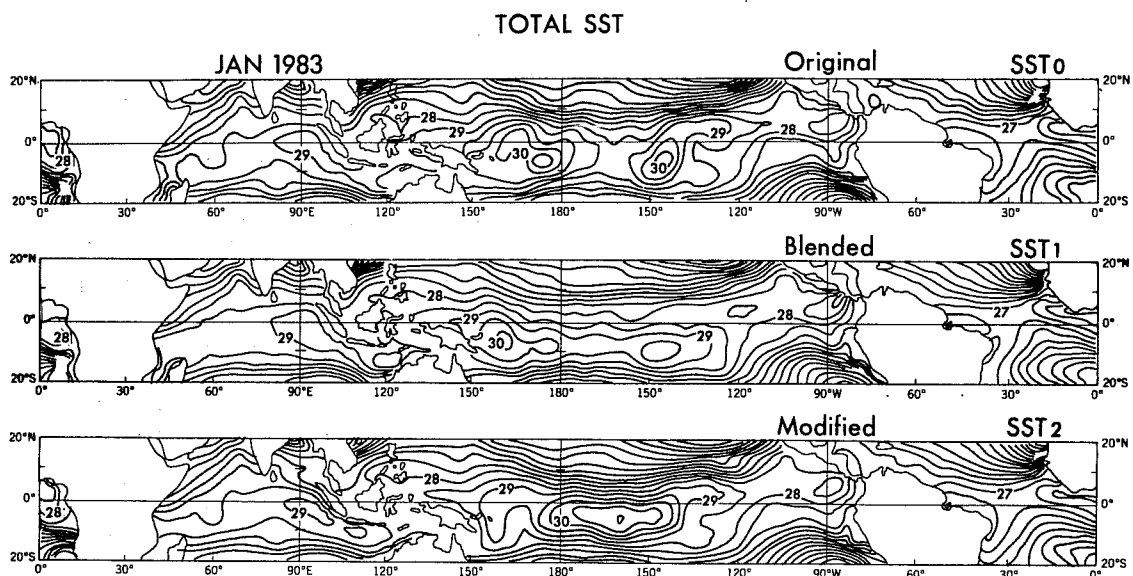
TOTAL SST

Fig. 14 Observed SST for January 1983 in units of degree Celsius. The contour interval is 5°C. See the text for three versions of SST.

form a maximum there, and in addition, the SST was reduced in the area of Indonesia-Australia where a substantial negative SST anomaly is expected in view of the suppressed rainfall.

The results of the forecasts using the FS-model and the NMC initial condition are shown in Figs. 15 and 16. As was speculated, the SST2 gave the best scores not only in the tropics, but also in the extratropics. This does not necessarily mean that the SST2 is correct, but it indicates that the delicate precision of tropical SST is influential for the mid-latitude circulation.

Our main concern, however, is item (a). There is a good reason why we suspect the adequacy of the initial conditions. Figure 17 displays the 60 day Hovmöller diagrams for the 5-day mean velocity potential at 200 mb (χ200) averaged from 8.4°N to 8.4°S. Three kinds of datasets are included in this figure – the observations (NMC analyses),the FM model prediction, and the FMS model prediction. The forecasts were performed using the ECMWF initial condition, starting from 00 GMT, 1 December 1982, and ending on 31 January 1983. In each panel, the 60-day mean of χ for the respective longitude has been removed. The slanting straight lines indicate 40-50 day wave propagation; the lines identified in the observation are copied on the diagrams of the FM and the FMS forecasts.

Inspection of this figure leads to the following conclusions: (a) The forecasts in the FM and the FMS are quite different from the observations, despite the fact that the χ-fields at Day 0 are similar to each other in the NMC and the ECMWF analysis (not shown here); (b) There is some evidence for eastward propagation of the χ patterns for both the observations and the forecasts; (c) The phases are different between the forecasts and the observations,and also the magnitude is much weaker in the forecasts; (d) The difference between the FM and the FMS is not large,

41

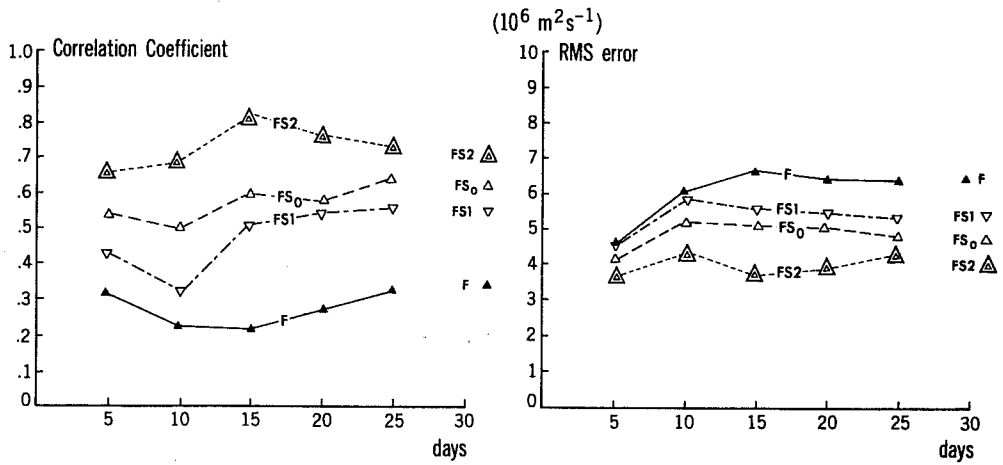χ 200   (NMC-IC)   JAN 1983   TROPICS (25°N-25°S)

Fig. 15 Skill scores of velocity potential χ at 200 mb in the tropics for four forecasts of four different SST. The correlation coefficients (left) and the rms error (right) of x in units of 10^6 m^2s^{-1}. The initial condition is the NMC analysis.

JAN 1983

Z 500
(NMC-IC)

NH (90°N-25°N)

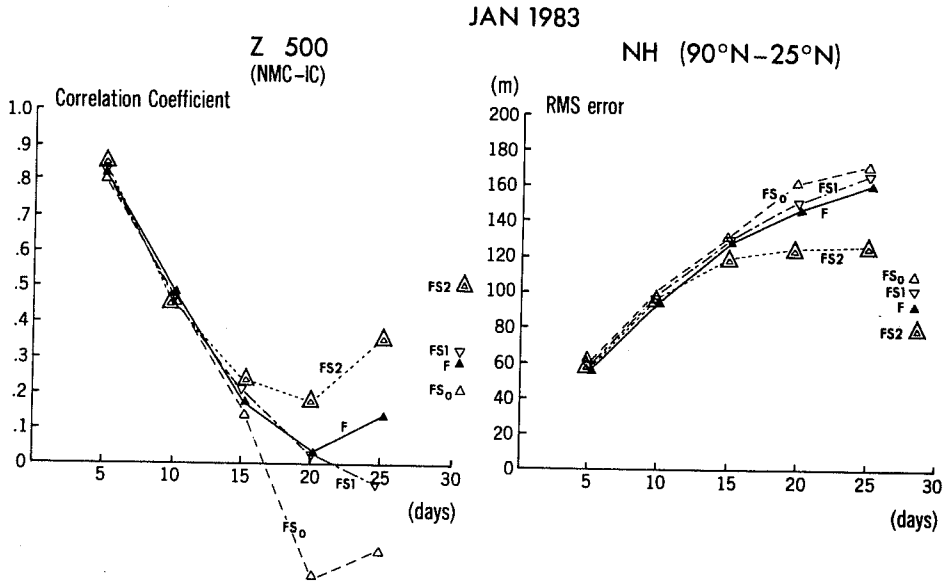

Fig. 16 Skill scores of the geopotential height at 500 mb in the extratropics for four different forecasts. See Fig.15 for further explanation.
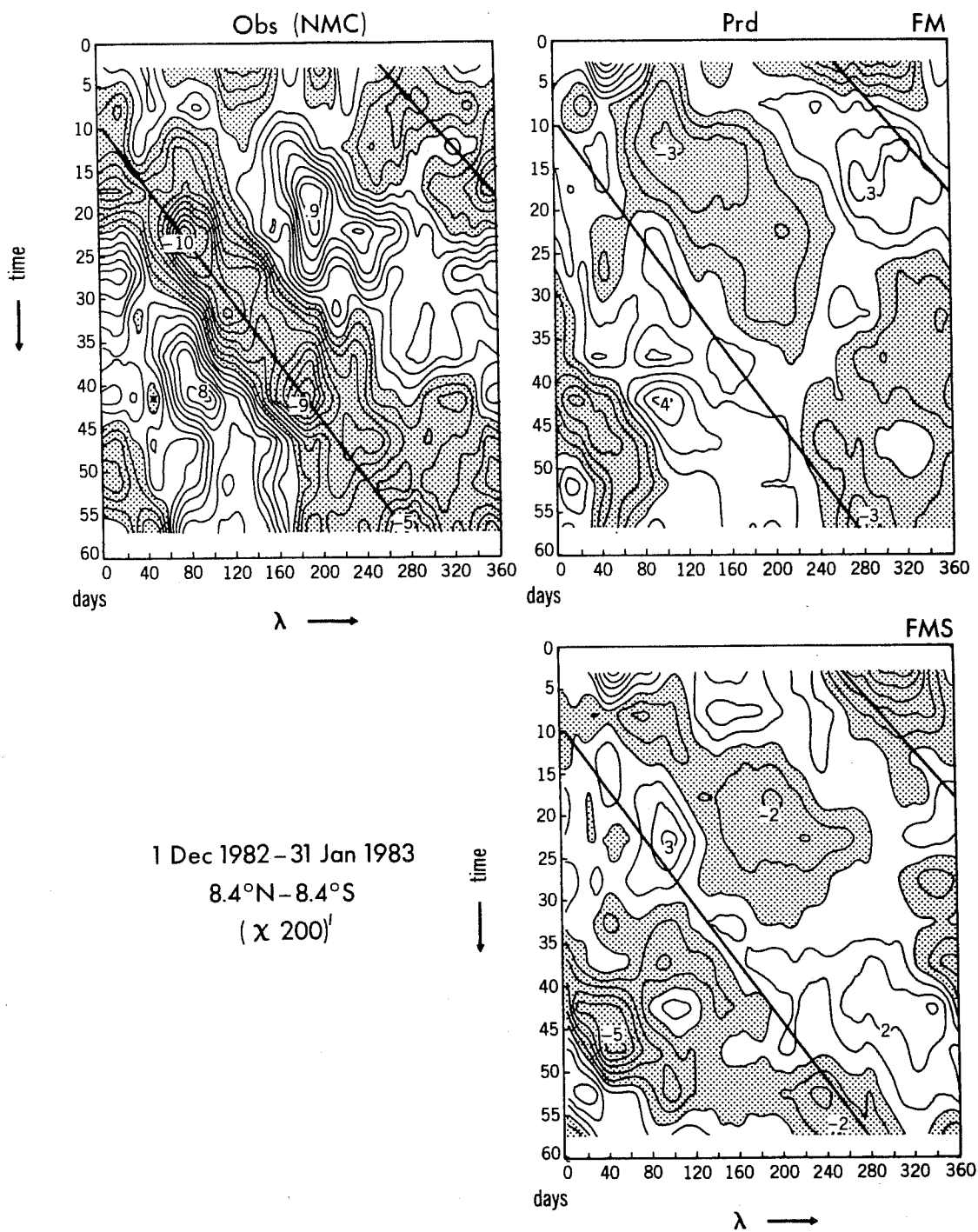
42

Obs (NMC)

Prd   FM

1 Dec 1982 – 31 Jan 1983

8.4°N – 8.4°S

(χ 200)^{I}

FMS

Fig. 17 Hovmöller diagram of the departure of the velocity potential χ at 200 mb from the 60 day mean at the respective longitudes. The χ is in units of 10^6 m^{2}s^{-1}; the negative regions are shaded. The observations (upper left), the FM forecasts (upper right), and the FMS forecasts (lower right). The ordinate is the forecasts time, starting from 00 GMT, 1 December 1982 to the subsequent 60 days. The abscissa is the longitude with the dateline at the middle.

implying that the SST effect is secondary, compared with the effect the 40-50 day oscillation; (e) At Day 60, the phases of the anomalies in the forecasts appear to agree with that in the observations.

The height-longitude structure of χ (not shown here) confirms the discrepancy between the observations and the forecasts. These facts indicate that the GCMs' solution underwent large changes in the transition from the initial time to the first several days and, as a result, phase information on the tropical 40-50 day waves was lost some time in this initial time of the forecast.

In real data, the 40-50 day waves are a very important mode of intraseasonal variability in the tropical circulation and are closely associated with fluctuations in large-scale cumulus convection. Figures 18a and 18b are the observed life cycle of the large-scale divergent wind fields represented by χ_{250} (250 mb) for the November through April season, and the corresponding convection pattern, as inferrred from the OLR satellite data (Knutson and Weickmann, 1986). The composits were derived from an EOF analysis of 30-60 day filtered χ data using NMC analyses for 1979-1985. Based on the first two principal components, which explain 39% and 33% of the 30-60 day variance, respectively, Knutson and Weickmann formed 12 composite categories of χ_{250} which describe the eastward propagation of the 40-50 day wave (Madden and Julian, 1971). Superimposed upon the patterns of χ_{250} anomalies in Fig. 18 are composite 30-60 day filtered OLR anomalies for the same time periods. Negative anomalies of more than 5 W·m^{-2} are indicated by the dark shading.

It is most striking that the OLR patterns are located near the centers of negative anomaly of χ_{250} (inferred rising motion) in all categories, and that both anomalies move together eastward around the globe at the speed of about 10 m·s^{-1}. The OLR anomalies become prominent over the Indian

44

Ocean region (category 11-12) before reaching their maximum spatial

extent over Indonesia and the South Pacific Convergence Zone (category

1-4). The OLR anomalies decay after passing the dateline (category 9),

then re-appear over the Indian Ocean (category 8-10) (see also Murakami,

1985, though the work is for northern hemisphere summer).

It has been widely believed that the 40-50 day waves are the consequence

of the interaction between equatorial waves and condensation, and that the

SST may determine the intensity of the convection anomalies but is not a

dominant propagation-producing mechanism for the 40-50 day oscillation.

In any case, the strong spatial association between the χ and OLR

anomalies suggests that the 40-50 day wave is very important in

determining the tropical condensation and accordingly the cumulus heating

on intra-seasonal time scales.

Turning back to the problem of extended-range forecasts, Puri (1985)

demonstrated that the gravity waves, particularly Kelvin waves, are the

major components of vertical motion generating tropical cumulus heating.

In particular, the low frequency Kelvin modes (slower than say 6 hours)

are most essential for causing condensation as well as evaporation, so

far as an adequate cumulus parameterization is used in GCMs. It has been

a long standing issue how the initial transition from the objective

analysis to the forecast can be adequately processed. If one starts the

forecasts from the gravity-lacking initial condition, it takes three days,

at least, to have a full spin-up of tropical rainfall (Miyakoda et al.,

1978; Puri, 1985; Heckley, 1986), but more importantly, the phase

information on the 40-50 day oscillation may be seriously disturbed.

Although our problem is related in a broad sense to the initialization, it

is, exactly speaking, how to handle the transition from the 4-dimensional

analysis to the forecast with a special emphasis on the preservation of
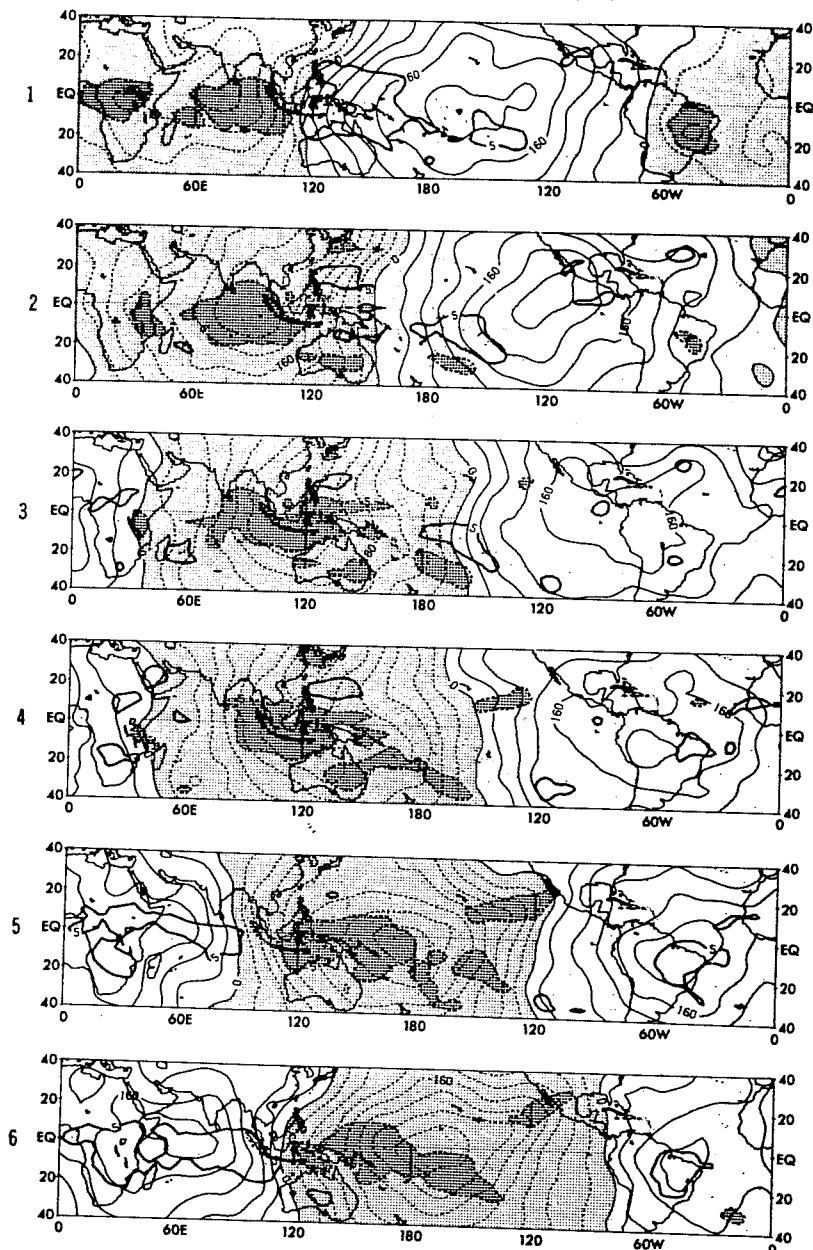
χ_{250} and OLR (November – April)

Fig. 18 Northern hemisphere winter composite χ at 250 mb anomalies (light contours and shading) with composite OLR anomalies of 5 W/m^2 or more superimposed (dark contours with dark shading for negative regions). Contour interval of χ is $4.0 \times 10^5 \ m^2/s$; negative values are shaded. (After Knutson and Weickmann, 1986).
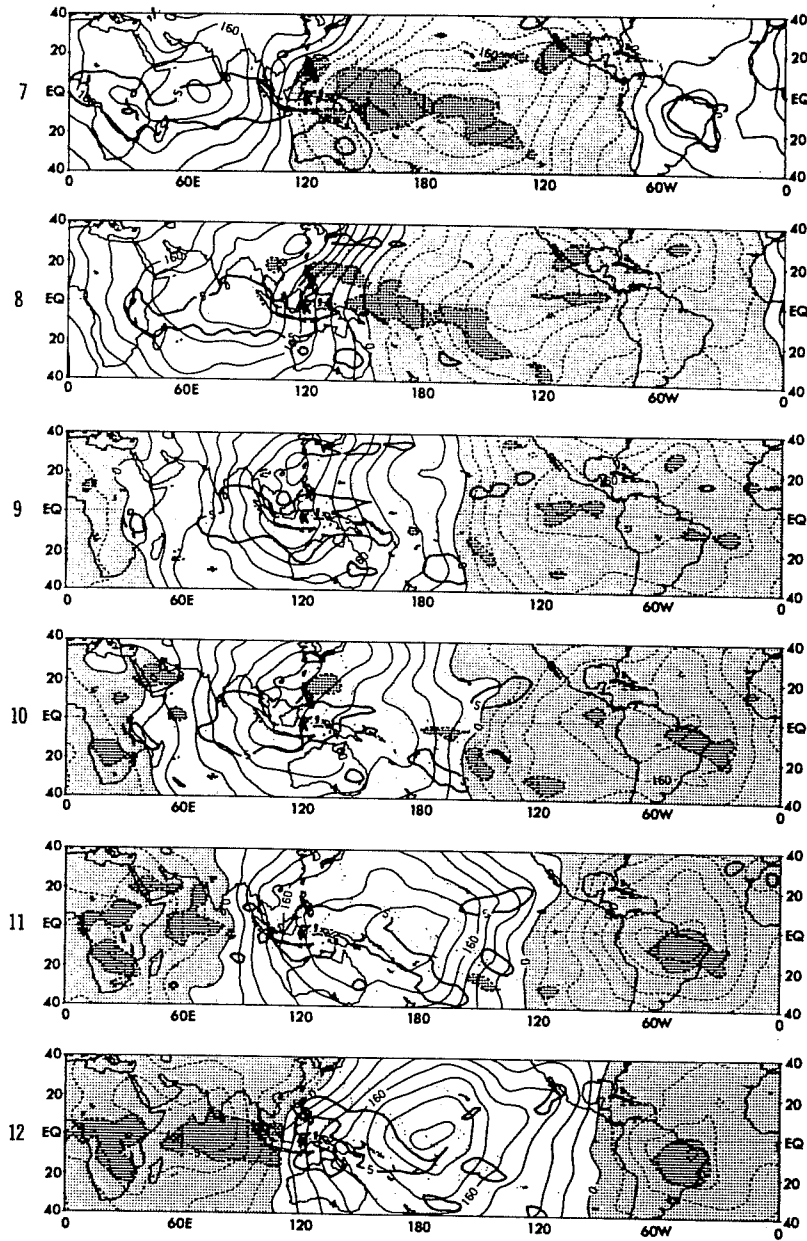
χ_{250} and OLR (November – April),

Fig. 18 (Continued)

these waves. The proper inclusion of the 40-50 day oscillation in the forecasting system may be a prerequisite for the adequate representation of the tropical SST effect.

In summary, the current GFDL forecasting system is impaired in representing the 40-50 day waves adequately, so generating the disarray of χ-fields in the initial stages of the forecasts which contributes to the poor response of the GCM to anomalous SSTs in the tropics.

8. CONCLUSIONS

(i)   The 30-day forecasts may be feasible.

(ii)   However, the systematic bias (climate drift) has to be removed for the outright application of dynamical forecasts.

(iii)   In the current GFDL model, the climate drift occupies 64% of the forecasts error for the 500 mb geopotential height, in the northern hemisphere extratropics. The climate drift of tropical of temperature at 300 mb constitutes 94% of the forecast error.

(iv)   In order to utilize the observed tropical SST effect for the mid-latitude forecasts, such problems as proper initialization of the 40-50 day oscillation and reduction of tropical climate drift will have to be addressed.

9. References

Arakawa, A., and W. H. Schubert, 1974: Interaction of cumulus ensemble with the large-scale environment. Part 1. _J. Atmos. Sci._, _31_, 674-701.

Bjerknes, J. 1969: Atmospheric teleconnections from the equatorial Pacific. _Mon. Wea. Rev._, _97_, 163-172.

Blackmon, M. L., J. M. Wallace, N.-C. Lau, and S. L. Mullen, 1977: An observational study of the northern hemisphere wintertime circulation. _J. Atmos. Sci._, _34_, 1040-1053.

Cubasch, U., and A. C. Wiin-Nielsen, 1986: Predictability studies with the ECMWF spectral model for the extended range: The impact of horizontal resolution and sea surface temperature. _Tellus_, _38A_, 25-41.

Fennessy, M. J., L. Marx, and J. Shukla, 1985: General circulation model sensitivity to 1982-83 equatorial Pacific sea surface temperature anomalies. _Mon. Wea. Rev._, _113_, 858-864.

Hayashi, Y., 1986: Statistical interpretations of ensemble-time mean predictability. _J. Meteor. Soc. Jap._, _64_, 167-181.

Heckley, W. A., 1984: Systematic errors of the ECMWF forecasting system in tropical regions _ECMWF Tech. Rep._ [Available at ECMWF, Shinfield Park, Reading, Berkshire, RG2 9AX, England.]

Kang, I.-S., and N.-C. Lau, 1986: Principal modes of atmopsheric variability in model atmospheres with and without anomalous sea surface temperature forcing in the tropical Pacific. _Mon. Wea. Rev,_ (submitted).

Knutson, T. R., and K. M. Weickmann, 1986: 30-60 day atmospheric oscillations: Composite life cycles of convection and circulation anomalies. _Mon. Wea. Rev._, (submitted).

Lau, N.-C., 1985: Modeling the seasonal dependence of the atmospheric response to observed El Niños in 1962-76. _Mon. Wea. Rev._, _113_, 1970-1996.

Madden R. A., 1976: Estimates of the natural variability of time-averaged sea-level pressure. _Mon. Wea. Rev._, _104_, 942-952.

Madden, R. A., and P. R. Julian, 1971: Detection of a 40-50 day oscillation in the zonal wind in the tropical Pacific. _J. Atmos. Sci._, _28_, 702-708.

Miyakoda, K., J. Sirutis, and J. Ploshay, 1986: One-month forecast experiments – without anomaly boundary forcings. _Mon. Wea. Rev._ (submitted).

Miyakoda, K., R. F. Strickler, and J. Chludzinski, 1978: Initialization with the data assimilation method. _Tellus_, _30_, 32-54.

Murakami, T., 1985: Tropical 45-day oscillations during the 1979 northern hemisphere summer. J. Atmos. Sci., 42, 1107-1122.

Palmer, T. N., and D. A. Mansfield, 1986: A study of wintertime circulation anomalies during past El Niño events using a high resolution general circulation model. II: Variability of the seasonal mean response. Quart. J. Roy. Meteor. Soc., 112, (in press).

Puri, K., 1985: Sensitivity of low-latitude velocity potential field in a numerical weather prediction model to initial conditions, initialization and physical processes. Mon. Wea. Rev., 113, 449-466.

Reynolds, R. W., 1982: A monthly averaged climatology of sea surface temperatures. NOAA Tech. Rep. NWS 31, Washington, D.C., 33 pp.

Reynolds, R. W., 1983: A comparison of sea surface temperature climatologies. J. Clim. Appl. Meteor., 22, 447-459.

Rowntree, P. R., 1972: The influence of tropical east Pacific Ocean temperature on the atmosphere. Quart. J. Roy. Meteor. Soc., 102, 607-625.

Shukla, J., 1981: Dynamical predictability of monthly means. J. Atmos. Sci., 38, 2547-2572.

Shukla, J., 1983: Comments on "Natural Variability and Predictability." Mon. Wea. Rev., 111, 581-585.

Sirutis, J., Y.-H. Lü, R. Reynolds, J. Ploshay, and K. Miyakoda, 1986: Simulation of the 1982/83 El Niño event: The atmospheric response for oceanic forcings. Mon. Wea. Rev., (to be submitted).

Wallace, J. M., S. Tibaldi, and A. J. Simmons, 1983: Reduction of systematic forecast errors in the ECMWF model through the introduction of an envelope orography. Quart. J. Roy. Meteor. Soc., 109, 683-717.

Webster, P. J., 1972: Response of the tropical atmosphere to local, steady, forcing. Mon. Wea. Rev., 110, 518-540.